Desalination and Water Treatment
www.deswater.com

doi: 10.5004/dwt.2023.29275

286 (2023) 1–15
February

Modeling and simulation of solar chimney/HWT power plant for the assistance of reverse osmosis desalination and electric power generation

A. Lilane[a,*], D. Saifaoui[a], S. Ettami[a], M. Chouiekh[a], Y. Aroussy[a], MA. Sharaf Eldean[b]

[a]*Laboratory of Renewable Energy and Dynamic Systems, Faculty of Sciences Aîn Chock, Hassan II University of Casablanca, El-Jadida Road km 9-BP 5366 Maarif Casablanca-Morocco, Tel.: +212(0)626 144 316; emails: amine.lilane-etu@etu.univh2c.ma/ m.amine.lilane@gmail.com (A. Lilane), ddsaifaoui@gmail.com (D. Saifaoui), ettamisaid@gmail.com (S. Ettami), chouiekh.mohamed@gmail.com (M. Chouiekh), aroussy110@gmail.com (Y. Aroussy)*
[b]*Department of Mechanical Engineering, Faculty of Engineering, Suez University, Egypt, email: mohammed.eldeen@suezuniv.edu.eg*

Received 10 June 2022; Accepted 19 December 2022

ABSTRACT

The world has currently recognized an essential technical and technological progress that has increased the lifespan of human beings and is one of the results of demographic evolution, which requires meeting the enormous energy and hydraulic needs of the population, especially in areas facing water stress. A novel reverse osmosis membrane desalination system engineering is presented and evaluated, using a Solar Chimney Power Plant (SCPP) and a Horizontal Wind Turbine (HWT). The proposed system is aimed to provide approximately 3,500–10,500 m^3/d of freshwater from seawater (salinity ratio = 40,000 ppm) and about 10 MWe of electricity. The freshwater produced is expected to serve around 55,000–100,000 inhabitants in a semi-arid area in Morocco and Kingdom of Saudi Arabia (KSA). Horizontal wind turbine and battery bank will be used as a backup source of power during the sun off periods. In this work, two different case studies that present two different regions are performed (North Africa and the Arabian Gulf regions). The results revealed that the specific power consumption is over 6.181 kWh/m^3.

Keywords: Reverse osmosis; Desalination; Renewable energy; Solar chimney; Horizontal wind turbine

1. Introduction

The water shortage problem is the main cause of many deaths and diseases in the last few decades. According to UNICEF [1], nearly 9 out of 10 children in the Middle East and North Africa (MENA) live in areas of high or extremely high-water stress with serious consequences on their health, nutrition, cognitive development, and future livelihoods. The MENA region is reported to be the most water-scarce region in the world. Nearly 66 million people in the region lack basic sanitation, and very low proportions of wastewater are adequately treated [1]. Therefore, the desalination technology can play an important role to solve the water shortage problem in the MENA region. Desalination can be classified into two major parts. The 1st part is membrane desalination, and the 2nd part is thermal desalination. However, desalination similar to any other technology needs power (thermal and/or electrical). Remarkably, MENA region has a great potential in energy resources especially renewable energy (solar and/or wind). For instance, and with respect to the solar energy example, the sunshine hours in the MENA region is about 3,600 h/y with an average solar radiation of 6–7 kWh/m^2 [2]. For that reason, desalination should be combined with renewable energies, particularly the solar energy. Many efforts have been considered in that regard especially in thermal desalination (multi-stage flash, multi effect distillation, and vapor compression) with solar energy [3–12]. However, membrane desalination such as reverse osmosis (RO) is considered

* Corresponding author.

as a vital option compared to thermal desalination while combining with renewable energies [13].

For instance, A.M. Soliman et al. [8], A.S. Nafey and M.A Sharaf [10], M.A. Sharaf [11], D.T. Agustín and G.R. Lourdes [14–16] have investigated the combination of solar organic Rankine cycle (ORC) and reverse osmosis desalination plant. Their results showed low specific power consumption and the availability of using solar thermal ORC with RO. For direct electrical combination between solar photovoltaic (PV), wind and RO, O. Charrouf et al. [17] investigated the effect of operating conditions (temperature, pressure, irradiation, etc.) on the system being studied. The total water price was about 0.25 $/m^3. A.A. Monjezi et al. [18] presented a thermal PV as a main power source for the RO unit. The specific consumption of the production plant energy was 0.12 kWh/m^3. W. Delgado et al. [19] optimized the solar micro grid for RO desalination process. X. Lai et al. [20] studied the use of mechanical and electrical combination between solar dish stirling and RO desalination, where the aim of this study was to improve the functional performance of desalination system. B. Martin-Gorriz et al. [21] presented a reverse osmosis desalination system coupled with a photovoltaic solar field where the objective was to integrate a new water treatment technique, and to reduce the overexploitation of aquifers in the field of greenhouse cultivation. A.S. Ibrahim et al. [22] investigated the integration of a photothermal reactor with the pre-treatment station. The system managed to reduce the total dissolved solids of the brine water from 18 to 70 mg/L, with an average rate of elimination of around 99.5% in climatic conditions close to that of standard temperature and pressure. S.E. Mohamed et al. [23] investigated technically and economically a photovoltaic powered brackish water reverse osmosis desalination system. This system was designed to produce an amount of 0.35 m^3/d with a specific power consumption of around 4.6 kWh/m^3. The main reason for the high cost of water production (15–20 €/m^3) was the need for solar batteries to achieve a constant pressure and flow rate for the membranes [23]. A.M. Helal et al. [24] studied the economic feasibility of driving RO by PV within low specific power consumption. Three alternative configurations of an autonomous PV-RO unit for remote areas in the United Arab Emirates (UAE) were investigated. They also studied the possibility of using a diesel generator for a day off periods. The PV-RO was not designed for more than 20 m^3/d (in 10 h). But they do not investigate the effect of diesel emissions on the environment. A. Cipollina et al. [25] presented and analyzed the operation of selected renewable energy system desalination unit, which demonstrated a productivity range from 1 to 10 m^3/d. Based on material effects on PV-RO, M. Freire-Gormaly and A. Bilton [26,27] presented an experimental investigation of the effect of intermittent operation characteristic of renewable powered desalination systems (PV-RO desalination). Their work showed a future work to develop robust design algorithms for renewable powered desalination systems. D. Manolakos et al. [28] presented some technical characteristics as well as an economic comparison of PV-RO desalination systems. The PV system was consisted of 18 arco-solar mono-crystalline PV panels, with total peak power of 846 W. Their system has a capacity of 0.1 m^3/h and the specific energy recovery of that system has been experimentally found to be in the range of 3.8–6 kWh/m^3. Their work estimated the cost at 7.77 €/m^3. But their work had not investigated the large-scale production based on the PV power. A.A. Hossam-Eldin et al. [29] studied a design of a PV powered by a small-scale reverse osmosis system. It was found that the cost of producing 1 m^3 of fresh water using the small PV powered RO water desalination systems is $3.73. E. Tzen et al. [30] studied that the design of an autonomous PV-RO system is able to cover potable and other water needs of a rural community in Morocco. That study was built based on 0.5 m^3/h powered by 7.5 kW of high-pressure pump power (SPC = 15 kWh/m^3) [30]. Another work was provided for wind powered RO. C.C.K. Liu et al. [31] presented a wind-driven reverse osmosis system for aquaculture wastewater treatment and demonstrated that freshwater can be used as a freshwater supply for fish culture [31]. The economic analysis was not investigated in the study of C.C.K. Liu et al. [31]. Operation of an experimental RO plant connected directly to a PV solar energy was studied by A. Lilane et al. [32], and the wind system without energy storage was studied by I.N. Pestana et al. [33]. The system was built to produce an amount of 3.6 m^3/h based on 21 kW of power. D.A. Dehmas et al. [34] studied the availability of using the wind power for seawater reverse osmosis (SWRO) desalination plant. An energy yield and economic analysis was performed on a hypothetical wind farm consisting of 5 of 2 MWe bonus wind turbines and determined that wind energy can successfully power an SWRO desalination plant. According to the literature, the majority of solar electrical RO systems operated at micro or low capacities and one of the most important reasons is the use of PV systems. Therefore, the solar chimney power plant (SCPP) could be another vital option to power the RO and to deliver a suitable power for the end user. SCPP can provide up to 100 MWe with LEC = 0.1 €/kWh [35], which is remarkably attractive. It would be a remarkable work to combine such solar technology with RO desalination process. In fact, there is a minor research activity in this regard, where the SCPP was treated as a solar still and power generator. For instance, K. Rahbar and A. Riasi [36] presented a SCPP for only 120 kW combined with PV. The PV produced about 419–420 kW of power. The solar chimney worked as a solar still for desalination [36]. C. Méndez and Y. Bicer [37] presented a proposal for the use of SCPP to produce 80 kW of power beside the operation of the multi-stage flash (MSF) for desalination purposes. Solar chimney is exploited in the MSF desalination process for high system efficiency and to produce about 600 m^3/d [37]. A. Alkhalidi and Y.K. Al-Jraba'ah [38] presented a solar chimney coupled with a parabolic solar concentrator. The solar concentrator was used with the objective of vaporizing the sea water. The production of distilled water was around 1.25 m^3/m^2/y. P. Rahdan et al. [39] presented a solo solar chimney to produce 0.598–0.6 m^3/d and still effect was used. Méndez and Bicer [40] presented a hybrid SCPP/HWT (horizontal wind turbine) for MSF and RO desalination. The system used the SCPP as a steam generator for the MSF. HWT was used separately to serve the RO desalination plant. The total production was about 4,500 m^3/d with high share percentage

(85%) on the RO/HWT side. It is clearly noticeable from the literature that the combination between RO and SCPP is rarely existed. In this work, a new study is introduced regarding to SCPP/HWT for seawater reverse osmosis desalination processes. SCPP is used as the main source of power instead of using PV or PV/HWT. HWT will be used as a backup system for more power generation. It is anticipated by the system to serve about 50,000 to 100,000 inhabitants for their freshwater and power needs (3,500–10,000 m^3/d and 10 MWe). The direct combination between SCPP and RO was not investigated before especially for large capacity operations. Meteorological data is also presented. The Mathematical and optimization models are performed as well. The system performance will be examined along the year under different operating conditions.

The objective of this paper is to analyze the potential electric energy production by SCPPT/RO in Casablanca, Morocco and Jeddah, KSA cities operating conditions (MENA and the Arabian Gulf regions) and to estimate the produced water. This production system can produce a quantity of water that can reach up to 13,810 m^3/d, with a power that can exceed 7 MW injected into the electricity grid in the sunniest areas. This study also presents an analysis about the influence of some geometrical and physical parameters, such as chimney height, collector diameter, ambient temperature, and solar radiation, on the power output of solar chimney power plants.

2. Novel system proposed

This part provides a complete and detailed description of the proposed system. Mathematical models, assumptions, and operating conditions are presented.

2.1. Process description

The novel system contains solar chimney power plant (SCPP) for electric power generation, horizontal wind turbine (HWT) for backup operation and power generation, and reverse osmosis (RO) for desalination purpose. Fig. 1 shows a schematic diagram of the proposed novel system. The SCPP or the solar updraft tower (SUT) is a design concept for a renewable-energy power plant for generating electricity from low temperature solar heat. Sunshine heats the air beneath a very wide greenhouse-like roofed collector structure surrounding the central base of a very tall chimney tower. The resulting convection causes a hot air updraft in the tower by the chimney effect. This airflow drives wind turbines, placed in the chimney updraft or around the chimney base, to produce electricity. The power output depends primarily on two factors: collector area and chimney height. During the sun off periods, HWT farm will be used to serve the loads (RO + user load demands). For RO part, the seawater is considered as the main feed to the RO stage. RO with basic stage will be considered in this work, that is, no energy recovery devices will be used.

2.2. Developed mathematical model

2.2.1. Solar chimney mathematical model

To calculate the performance and energy streams across the SCPP [35,41–44], the mean air temperature (°C) is calculated as follows: where T_{amb} is the ambient air temperature, and T_{ai} is the air temperature entering to the chimney, °C.

$$T_{am} = \frac{T_{amb} + T_{ai}}{2} \quad (1)$$

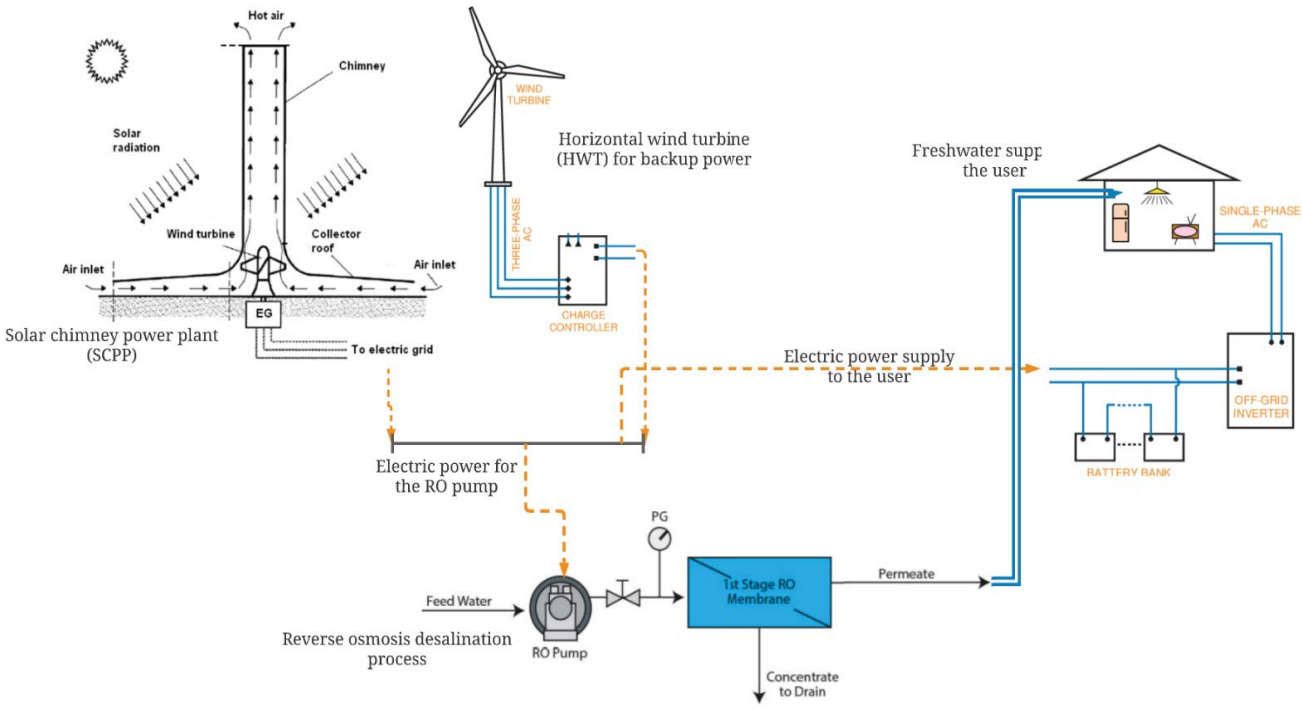

Fig. 1. A schematic diagram of the novel system proposed for seawater desalination (RO) and power generation (SCPP/HWT).

The total solar field area, m² is calculated based on the field diameter, D_{col}, m:

$$A_{col} = \frac{\pi}{4} D_{col}^2 \tag{2}$$

The chimney cross sectional area, m² is calculated based on the chimney diameter, m:

$$A_{ch} = \frac{\pi}{4} D_{chi}^2 \tag{3}$$

Chimney diameter difference, m, where D_{cho} and D_{chi} are the outlet and inlet chimney diameter, respectively:

$$d_r = D_{cho} - D_{chi} \tag{4}$$

Air velocity at the chimney entrance, m/s, where H_{ch} is the chimney height, m:

$$V_{air} = \sqrt{2 \times 9.81 \times H_{ch} \times \frac{T_{ai} - T_{amb}}{T_{amb} + 273.5}} \tag{5}$$

The mass of air at chimney entrance, kg/s:

$$M_{air} = \rho \times A_{ch} \times V_{air} \tag{6}$$

The mass of air through the collector, kg/s is calculated based on the mass balance across all system:

$$M_{ac} = M_{air} \tag{7}$$

Hence, the air velocity through the collector, m/s is calculated based on the air density, area and mass flow rate:

$$V_{ac} = \frac{M_{ac}}{\rho \times A_{col}} \tag{8}$$

The pressure difference d_p is produced between tower base (collector outlet) and the ambient, Pa:

$$dP = 9.81 \times \left(\rho\left(T_{amb}\right) - \rho\left(T_{air}\right)\right) \times H_{ch} \tag{9}$$

Then, the chimney power, W can be calculated:

$$P_{ch} = dP \times V_{air} \times A_{col} \tag{10}$$

Useful air thermal power, W:

$$Q_a = M_{air} \times C_{pa}\left(T_{am}\right) \times \left(T_{air} - T_{amb}\right) \tag{11}$$

The chimney efficiency is then calculated based on the chimney power and air thermal power:

$$\eta_{ch} = \frac{P_{ch}}{Q_a} \tag{12}$$

For the electric part in the SCPP, the turbine rotor area, m² is calculated based on rotor diameter, m:

$$D_r = D_{chi} \tag{13}$$

$$A_r = \frac{\pi}{4} D_r^2 \tag{14}$$

The air speed through the rotor, m/s is calculated based on the rotor area and mass flow rate of the air through the rotor, kg/s:

$$V_r = \frac{M_{air}}{A_r \times \rho\left(T_{am} + 273\right)} \tag{15}$$

To calculate the collector efficiency, thermal loss should be calculated. The radiation lose to the ambient from the collector, W/m²·K:

$$Q_{r\_a} = E_c \times \sigma \times A_{col} \times \left(\left(T_{ai} + 273\right)^4 - \left(T_{amb} + 273\right)^4\right) \tag{16}$$

The convection heat transfer coefficient from the collector to the ambient, W/m²·K:

$$h_{c\_a} = 3.87 + 0.0022 \times \frac{V_{ac} \times \rho\left(T_{am}\right) \times C_{pa}\left(T_{am}\right)}{2/3 \times P_r\left(T_{am}\right)} + \left(2.2 \times V_w + 8.3\right) \tag{17}$$

The overall heat transfer coefficients between collector and ambient, W/m²·K:

$$U_l = \frac{1}{\left(1/h_{c\_a}\right) + \left(D_c / kc\right)} \tag{18}$$

Another expression of the overall losses can be expressed from the overall energy balance of the whole system.

$$U_l = \left(\frac{I_s \times \left(1 - \eta_t\right)}{\Delta T}\right) - \left(\frac{D_{ch}}{D_c}\right)^2 \times \rho_a \times C_{pa} \times \sqrt{2 \times 981 \times H_{ch} \times \frac{\Delta T}{T_{amb}}} \tag{19}$$

The conduction loss from the chimney, W, where k_{ch} is the thermal conductivity, W/m·K:

$$Q_{lch} = k_{ch} \times A_{ch} \times \frac{T_{ai} - T_{amb}}{d_r} \tag{20}$$

The thermal total loss power through the collector and chimney tower, W:

$$Q_l = \left(U_l \times A_{col} \times \left(T_{air} - T_{amb}\right)\right) + Q_{lch} + Q_{r\_a} \tag{21}$$

The solar thermal power, W:

$$Q_s = I_s \times A_{\text{col}} \times \alpha_c \tag{22}$$

The collector efficiency:

$$\eta_{\text{col}} = \frac{Q_a}{Q_s} \tag{23}$$

The total plant efficiency:

$$\eta_t = \eta_{\text{col}} \times \eta_{\text{ch}} \times \eta_t \tag{24}$$

The net power from the SCPP, W:

$$P_{\text{net}} = \left(Q_s - Q_l\right) \times \eta_t \tag{25}$$

2.2.2. HWT mathematical model

The HWT mathematical model used in this study is given by following equations [45,46]:

Air density kg/m^3 at sea level is calculated based on air temperature, °C, and site elevation, H_s, m:

$$T_{\text{air}} = 15.5 - \left(19.83 \times \frac{H_s}{3{,}048}\right) \tag{26}$$

$$\rho_{\text{air}} = \frac{\left(P_{\text{air}} \times 100\right)}{0.287 \times \left(T_{\text{air}} + 273.15\right)} \times e^{\left(-1 \times 0.297 \times \frac{H_s}{3048}\right)} \tag{27}$$

The HWT rotor swept area m^2:

$$A_r = \frac{\pi}{4} \times D_r^2 \tag{28}$$

Air mass flow rate kg/s:

$$M_{\text{air}} = \rho_{\text{air}} \times A_r \times V_{\text{wr}} \tag{29}$$

Wind speed at the blades, m/s where V_{wr} is the rated wind speed, m/s, and ASR is the air speed ratio (=4 for 3 blades type):

$$V_u = \frac{V_{\text{wr}}}{\text{ASR}} \tag{30}$$

Power coefficient:

$$C_P = \frac{4 \times V_{\text{wr}}^2}{V_u^2} \times \left(1 - \frac{V_{\text{wr}}}{V_u}\right) \tag{31}$$

The required wind power, kW:

$$\text{HP}_w = \frac{0.5 \times \rho_{\text{air}} \times A_r \times V_{\text{wr}}^3}{1{,}000} \tag{32}$$

The power delivered by the turbine, kW:

$$\text{HP}_{\text{mec}} = \text{HP}_w \times C_P \tag{33}$$

Rotor speed, RPM$_r$ is calculated based on the tip speed ratio (TSR) and rated wind speed, m/s:

$$\text{RPM}_r = \frac{\text{TSR} \times 60 \times V_{\text{wr}}}{\pi D_r} \tag{34}$$

Rotor torque N·m:

$$T_r = \frac{1{,}000 \times \text{HP}_{\text{mec}}}{\frac{2\pi \times \text{RPM}_r}{60}} \tag{35}$$

Power outlet from HWT generator, kW:

$$P_{\text{go}} = \eta_g \times \text{HP}_{\text{mec}} \tag{36}$$

Output current, A, where FP is the power factor lag and equal to 0.8:

$$I_g = \frac{1{,}000 \times P_{\text{go}}}{V\sqrt{3} \times \text{FP}} \tag{37}$$

Net power developed, kW:

$$P_{\text{nd}} = \text{HP}_{\text{mec}} - \left(\text{RL} \times P_{\text{go}}\right) \tag{38}$$

where RL is the rotational loss and equal to 0.11–0.12.

The total wind farm power (TFP), kW:

$$\text{TFP} = P_{\text{nd}} \times N_{\text{wt}} \tag{39}$$

where N_{wt} is the total number of wind turbines.

For the battery in discharging mode, AH should be calculated. For single battery, the AH$_b$ is calculated based on battery current, I_b, Amp, and the discharging time, t_d, h.

$$\text{AH}_b = I_b \times t_d \tag{40}$$

For single battery storage, Wh, the battery voltage V_b is multiplied by the AH$_b$.

$$\text{BSp} = \text{AH}_b \times V_b \tag{41}$$

Single battery power, W:

$$\text{Bp} = \frac{\text{BSp} \times \text{DOD} \times \eta_b}{\text{OH} \times \text{NOC}} \tag{42}$$

where, DOD is the battery depth of discharge and OH is the operating hours, h, and NOC is the number of cloudy days. The total battery power bank, W can be obtained based on the battery power, Bp and the number of batteries, NOB.

$$\mathrm{TBP} = \mathrm{Bp} \times \mathrm{NOB} \tag{43}$$

Load current, Amp can be obtained based on the total battery power and the load voltage based on the application.

$$I_l = \frac{\mathrm{TBP}}{V_l} \tag{44}$$

For charging mode, the same sequence will be considered, however, the charging time, t_c, h, will be assigned for the AH_b calculation.

Single battery Amp hour, AH.

$$\mathrm{AH}_b = I_b \times t_c \tag{45}$$

2.2.3. RO mathematical model

In desalination systems, where the reverse osmosis membrane is the heart of the whole project, overcoming the filtration resistance and the osmotic pressure of the membrane system is very important to force the solid-liquid filtration phenomenon. The fresh water is produced through the application of high pressure in the supply side by the high-pressure motor pump according to the configuration of the RO membrane unit in addition to the quality and quantity of the production [9,11,47]. The following figure (Fig. 2) shows the principle of a RO module. The RO model can be expressed based on the performance technique of modelling where the output productivity should be calculated based on the input power to the RO [48–51]. The feed flow rate, kg/s is calculated based on power load on the high-pressure pump (HPP, kW), the density, pump efficiency, and the pressure difference across the pump.

$$M_f = \frac{\mathrm{HPP} \times \rho\left(T, X_f\right) \times \eta_p}{\Delta P} \tag{46}$$

The RO productivity, kg/s is then calculated based on the assigned recovery ratio (RR) as follows:

$$M_p = \mathrm{RR} \times M_f \tag{47}$$

The product salt concentration, g/kg is then calculated based on the feed salinity ratio, X_f, g/kg and the salt rejection percentage (SR = ~0.98).

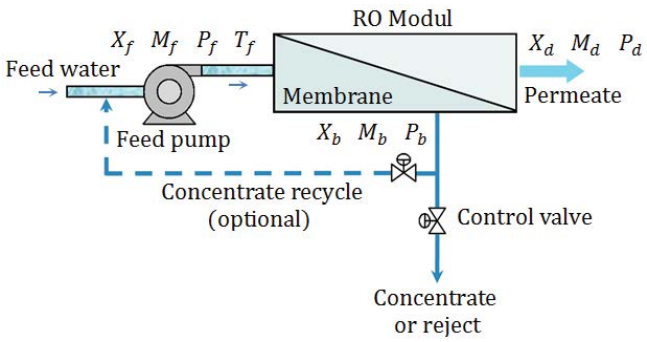

Fig. 2. Simplified basic flow diagram for the RO process.

$$X_p = X_f \times \left(1 - \mathrm{SR}\right) \tag{48}$$

The rejected brine kg/s is the difference between the feed flow rate and the product flow rate as follows:

$$M_b = M_f - M_p \tag{49}$$

Based on the mass and salt balances, the rejected salt concentration g/kg is then calculated.

$$X_b = \frac{M_f \times X_f - M_p \times X_p}{M_b} \tag{50}$$

The average salt concentration kg/m^3:

$$X_{\mathrm{av}} = \frac{M_f \times X_f + M_b \times X_b}{M_f + M_b} \tag{51}$$

The temperature correction factor, °C:

$$\mathrm{TCF} = \exp\left(2{,}700 \times \left(\frac{1}{T + 273} - \frac{1}{298}\right)\right) \tag{52}$$

The membrane water permeability k_w;

$$k_w = 6.84 \times 10^{-8} \times \frac{\left(18.6865 - \left(0.177 \times X_b\right)\right)}{\left(T + 273\right)} \tag{53}$$

The salt permeability k_s is:

$$k_s = \mathrm{FF} \times \mathrm{TCF} \times 4.72 \times 10^{-7} \times \left(0.06201 - \left(5.31 \times 10^{-5} \times \left(T + 273\right)\right)\right) \tag{54}$$

where FF is the membrane-fouling factor (FF = 0.8). The calculations of osmotic pressure for feed side, brine side, and distillate product side are found as follows:

$$\Pi_f = 75.84 \times X_f \tag{55}$$

$$\Pi_b = 75.84 \times X_b \tag{56}$$

$$\Pi_d = 75.84 \times X_d \tag{57}$$

The average and net osmotic pressure are then calculated:

$$\Pi_{\mathrm{av}} = 0.5 \times \left(\Pi_f + \Pi_b\right) \tag{58}$$

$$\Delta\Pi = \Pi_{\mathrm{av}} - \Pi_d \tag{59}$$

The net pressure difference across the membrane:

$$\Delta P = \left(\frac{M_d}{3{,}600 \times \mathrm{TCF} \times \mathrm{FF} \times A_e \times n_e \times N_v \times k_w}\right) + \Delta\Pi \tag{60}$$

where A_e is the element area in m², n_e is number of membrane elements, and N_v is the number of pressure vessels. The specific power consumption (SPC, kWh/m³) is then calculated based on the high-pressure pump (HPP, kW).

$$\mathrm{SPC} = \frac{1{,}000 \times \mathrm{HPP}}{3{,}600 \times M_p} \tag{61}$$

Density, kg/m³ is calculated as presented in the following function. This equation is applicable in the salinity range of 0 to 160 g/kg and for temperature from 10°C to 180°C.

$$\rho_w = \begin{pmatrix} 0.5 \times a_0 + a_1 \times Y + a_2 \times \left(2 \times Y^2 - 1\right) \\ + a_3 \times \left(4 \times Y^3 - 3 \times Y\right) \end{pmatrix} \times 1{,}000 \tag{62}$$

where,

$a_0 = 2.01611 + 0.115313 \times \sigma + 0.000326 \times ((2 \times (\sigma^2)) - 1)$;
$a_1 = -0.0541 + 0.001571 \times \sigma + 0.000423 \times ((2 \times (\sigma^2)) - 1)$
$a_2 = -0.006124 + 0.00174 \times \sigma + 0.000009 \times ((2 \times (\sigma^2)) - 1)$
$a_3 = 0.000346 + 0.00008 \times \sigma + 0.000053 \times ((2 \times (\sigma^2)) - 1)$

$$Y = \frac{2 \times T - 200}{160}, \sigma = \frac{\left(2{,}000 \times S\right) - 150}{150}, S\left[\mathrm{g/kg}\right]$$

Specific heat capacity (J/kg·°C): the specific heat of water at constant pressure is:

$$C_p = \frac{1}{1{,}000} \times \left(a_p + b_p \times T + c_p \times T^2 + d_p \times T^3\right) \tag{63}$$

$a_p = 4{,}206.8 - 6.6197 \times X + 1.2288 \times 10^{-2} \times X^2$;
$b_p = -1.1262 + 5.4178 \times 10^{-2} \times X - 2.2719 \times 10^{-4} \times X^2$;
$c_p = 1.2026 \times 10^{-2} - 5.3566 \times 10^{-4} \times X + 1.8906 \times 10^{-6} \times X^2$;
$d_p = 6.8774 \times 10^{-7} + 1.517 \times 10^{-6} \times X - 4.4268 \times 10^{-9} \times X^2$

2.3. Developed model browser

Engineering process consist of several interactive units, generally, to understand the behavior of these processes under different operating conditions, a flexible and general computer program is needed to simulate and control many flow sheeting processes. These processes can mostly be divided into two classes: (i) performance processes (current work), and (ii) design processes. In the performance problem, the variables are associated with the feed streams to a processing unit and all design parameters (such as solar field area, tower height dimensions, etc.) are assumed to be known.

The variables associated with the internal and output streams are unknown. To model and simulate the proposed system, a software program is quite essential to achieve that target. Matlab/Simulink has been used for that purpose. Based on the performance technique of modelling, the model will calculate the efficiency and power output from the SCPP/HWT/Battery. The power will drive on the high-pressure pump of the RO beside the load demand from the user (Table 1).

2.4. Description of the sites studied

In this section, Fig. 3 Represents the monthly average of solar radiation GHI, W/m² and wind speed, m/s for Casablanca, Morocco and Jeddah, KSA locations. According to Fig. 3a, the values of the monthly average solar radiation GHI of Jeddah, KSA are very important compared to that of Casablanca, Morocco, it recognizes an important value of the order of 960 W/m² (July), compared to a value of 850 W/m² which was recorded in Casablanca, Morocco as a maximum value mentioned in the same month (July). For this reason, it is noticeable that Jeddah, KSA represents a more efficient solar field compared to that of Casablanca, Morocco. According to Fig. 3b, the values of the monthly average wind speed of Casablanca, Morocco and Jeddah, KSA variants significantly throughout the year, in the periods of January–April, May–August and November–December the wind speed of Jeddah, KSA is higher than that of Casablanca, Morocco, on the other hand in the period of April–May and August–November, the average wind speed of the city of Casablanca, Morocco is the highest compared to that of Jeddah, KSA, the maximum average value of the wind speed is recorded in Jeddah (4.7 m/s in the month of June), this city also recognizes the minimum average value of the wind speed (3.15 m/s) which has been recorded in the month of October, it shows that the average wind speed in this city is not stable.

3. Results and discussion

Fig. 4 illustrates the performance results of the SCPP according to Casablanca and Jeddah locations during the whole year; it is the inlet chimney temperature (°C), the pressure drop (kPa), the total SCPP efficiency, the tower efficiency, the collector efficiency and the heat transfer losses (W/m²·K). According to Fig. 4a, the inlet chimney temperature, in Jeddah is very high compared to Casablanca throughout the year, especially in July with a temperature exceeding 60°C, this temperature variation is largely linked to the global irradiation of the studied region, practically, they have the same variation profile, in fact, the pressure drop in Jeddah is very high throughout the year compared to that of Casablanca. The total SCPP efficiency, in the periods between June–May and July–November, the efficiency in the region of Casablanca is very important compared to Jeddah, this efficiency varies between 58.5% in June and 61.5% in November (Fig. 4b). In other periods (May–July and November–December), the total return of SCPP is high in Jeddah, it varies between 58% in June and 62% in December. Regarding the tower efficiency, Fig. 4d shows perfectly that the tower performance in Casablanca city is higher than that of Jeddah throughout the year, especially in the period July–December, therefore the tower efficiency in Casablanca varies between 76.75% in June–July and 78.80% in December, on the other hand the collector efficiency in Casablanca and Jeddah represents a very high value, it varies between 90% and 98% (Fig. 4e). From a thermal transfer point of view, the SCPP lost thermal energy by convective effect, Fig. 4f shows clearly that the heat loss flux is essentially outstripping the wind speed of the studied site (Fig. 3b), consequently, a high wind speed, leading to a high heat transfer loss and vice versa. For this reason, the heat transfer loss in Jeddah are high compared to that of Casablanca because the average wind speed in Jeddah is high.

Fig. 5 represents the performance results through the SCPP according to Casablanca and Jeddah locations during

Table 1
Assigned data for the proposed system SCPP/HWT/RO

Process	Assigned parameters	References
RO	- Seawater salinity ratio = 40,000 ppm - Pressure drop = 4,000–7,000 kPa - Recovery ratio = 15%–30% - Number of pressure vessels = 75 - Number of elements per pressure vessel = 7 - Membrane area = 35.3 m^2	[9] [11] [47] [48] [49]
	SCPP	
SCPP	- Ambient temperature = 15°C–35°C - Solar radiation = 100–1,000 W/m^2 (vary based on the location) - Collector diameter = 250 m - Collector cover thickness = 0.02 m - Collector cover absorptivity = 0.89 - Collector cover emissivity = 0.88 - Collector cover conductivity = 0.03 W/m·K - Chimney height = 65 m - Chimney inner/outer diameter = 10/10.2 - Chimney thermal conductivity = 0.28 W/m·K - Chimney wind turbine and generator efficiency = 0.8 - Efficiency (mechanical) = 95%	[35] [41] [42] [43] [44]
	HWT	
HWT	- Ambient pressure = 1.03 bar - Ambient temperature=15°C–35°C - Wind speed = 2.5–15 m/s (vary based on the location) - Site friction factor = 0.2 - Site elevation = 100 m - Tip speed ratio = 4 - Air speed ratio=0.3–0.5 - Rotor diameter = 65 m - Number of HWT = 50 - Generator mechanical efficiency = 0.85 - Rotation loss = 0.11 - Power factor lag = 0.8	[45] [46]

the whole year; it is the net power (kW), the thermal power (kW), the air velocity at the turbine rotor (m/s), and the air mass flow rate (kg/s). According to Fig. 5a, the SCPP net power in Jeddah is higher compared to that of Casablanca, in fact, the Jeddah site has a net power of the order of 12 MW in July the irradiation is maximum. For Casablanca, the site has a net power of around 10 MW in June as its maximum value throughout the year. This energy production is just the results of the thermal power recovered by the SCPP, consequently, the site of Jeddah city represents a very high thermal power by contribution to Casablanca (Fig. 5b), a maximum value that exceeds 25 MW was recorded in Jeddah in July, and a minimum order value of 0.75 MW in December. In Casablanca city, the thermal power recovered by the SCPP varies between 0.4 MW in December and 2.25 MW in June. The power recovered as a contribution to the solar system has a perfect influence on the air speed at the level of the electric rotor production turbine, where the high thermal power (significant irradiations) influences the speed of the air that will cross the turbine is also becoming important. For this reason, the air speed at Jeddah site is higher than that of Casablanca throughout the year, the maximum value of this speed was recorded in Jeddah (~20 m/s in July), on the other hand, the Casablanca city site recognizes a minimum air speed (~11 m/s in December) throughout the year. These results will imperatively influence the air mass flow rate of the solar system (Fig. 5d), consequently, the air mass flow rate in Jeddah varies between 600 kg/s in December and exceeds 900 kg/s in July, for Casablanca, the air mass flow rate also varies from 500 kg/s in December to 890 kg/s in June, this variation mainly influences the rotation speed of the SCPP turbine, and consequently, the net production of the global power of SCPP (Fig. 5a).

Fig. 6 represents the performance results of the HWT farm according to Casablanca and Jeddah locations during the whole year; it is the turbine blades (m/s), the total farm

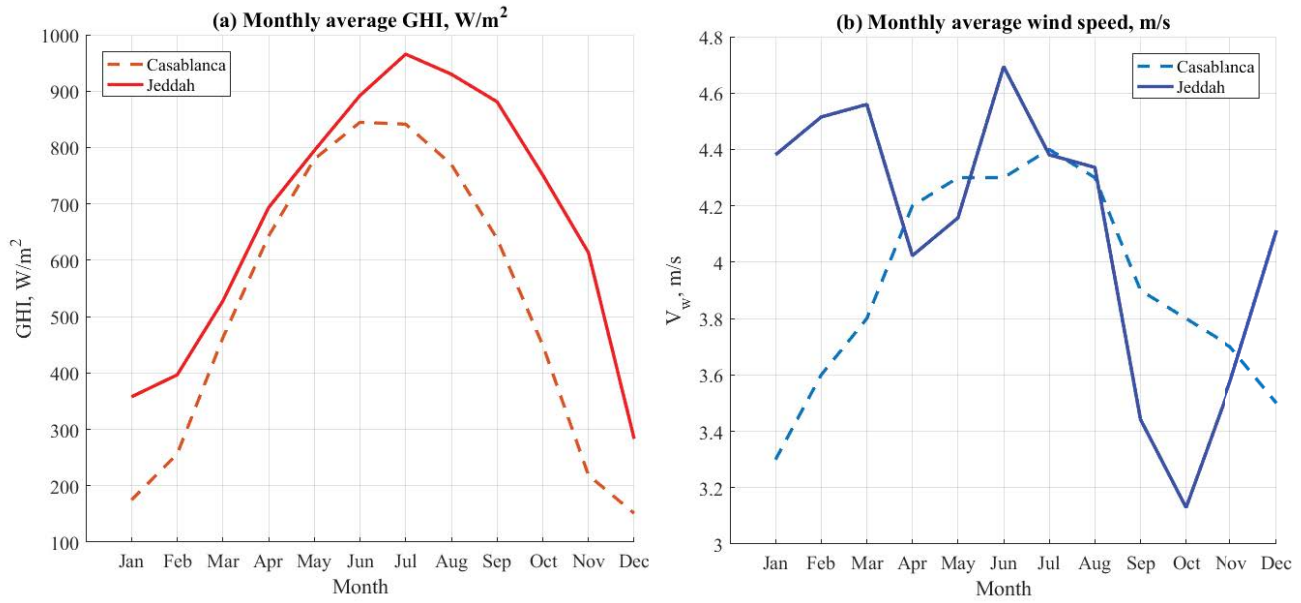

Fig. 3. Monthly average (a) solar radiation GHI and (b) wind speed for Casablanca, Morocco and Jeddah, KSA locations.

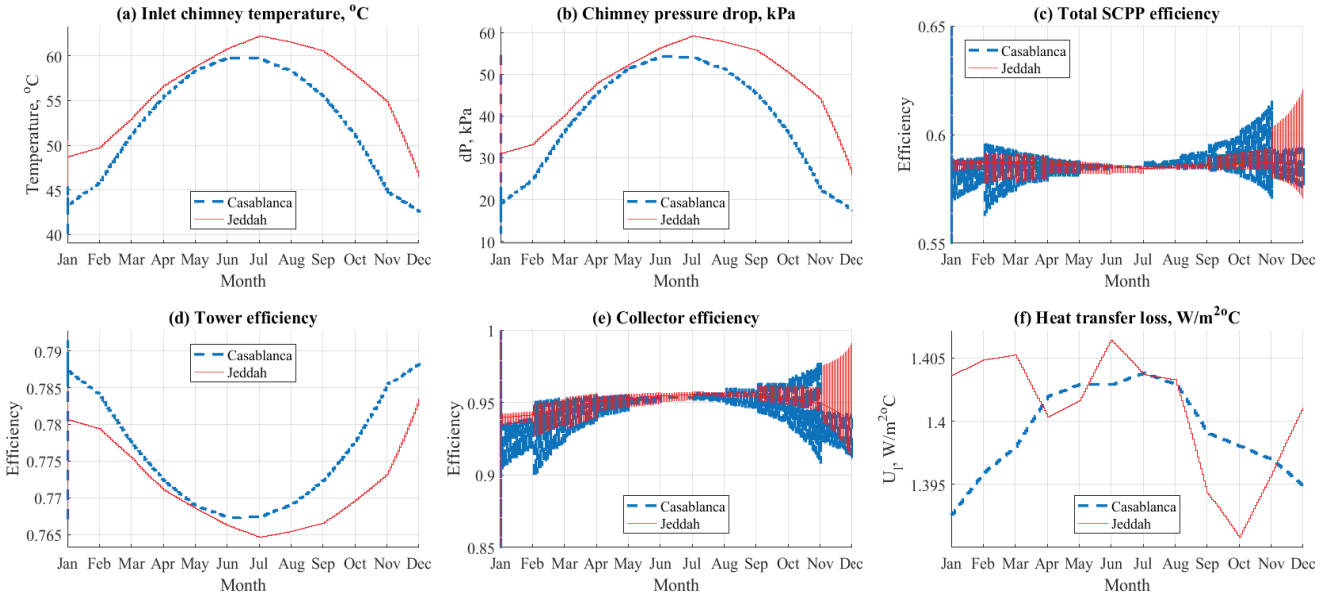

Fig. 4. Performance results of the SCPP according to Casablanca and Jeddah locations: (a) inlet chimney temperature, (b) pressure drop, (c) total SCPP efficiency, (d) tower efficiency, collector efficiency, and (f) heat transfer loss.

power (kW), the average generator power/module (kW), and current/module (A). According to Fig. 6a, the turbine blades are essentially dependent on the wind speed (Fig. 3a), in Jeddah city, it varies between 24 m/s in October and 36 m/s in June, with high disturbance throughout year. In Casablanca city, the turbine blades vary between 25 m/s in January and 34 m/s in July. These results will impact the power delivered by the wind farm (Fig. 6b), in fact, the maximum power value of the HWT farm was recorded in June in Jeddah, this value exceeds 2.7 MW, the same site has also a minimum production of the farm throughout the year (0.5 MW). In this performance study, the HWT farm is made up of 50 wind turbines (in Casablanca and Jeddah locations), and it is estimated that all wind turbines operate under the same conditions, and produce same elementary power during the operating period, according to Fig. 6c, each wind turbine in Casablanca produces power that varies between 200 and 475 kW throughout the year, and between 100 and 575 kW in Jeddah during the same period of operation. Consequently, the current generated by each wind turbine also varies according to the variation in the power produced (Fig. 6d). Therefore, the elementary current generated in Casablanca varies between 680 and 1,580 A, and between 560 and 1,920 A in Jeddah.

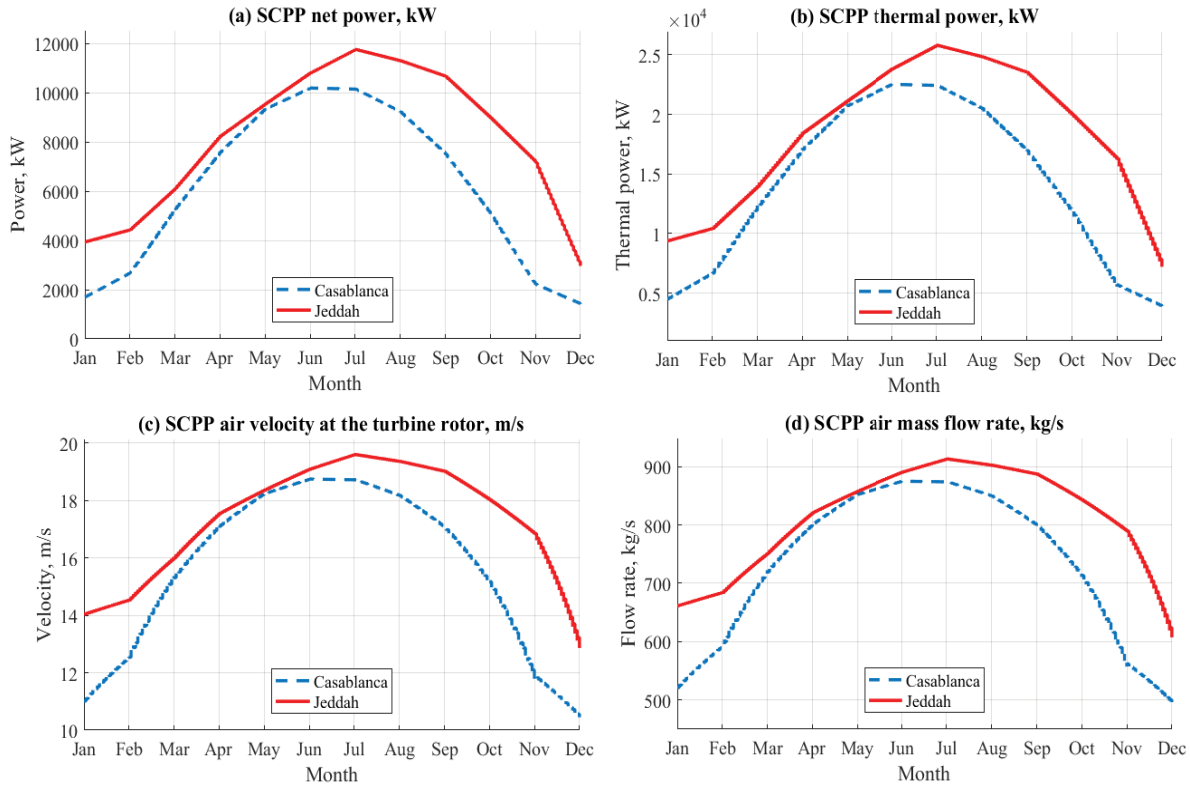

Fig. 5. Power and air velocity performance through the SCPP.

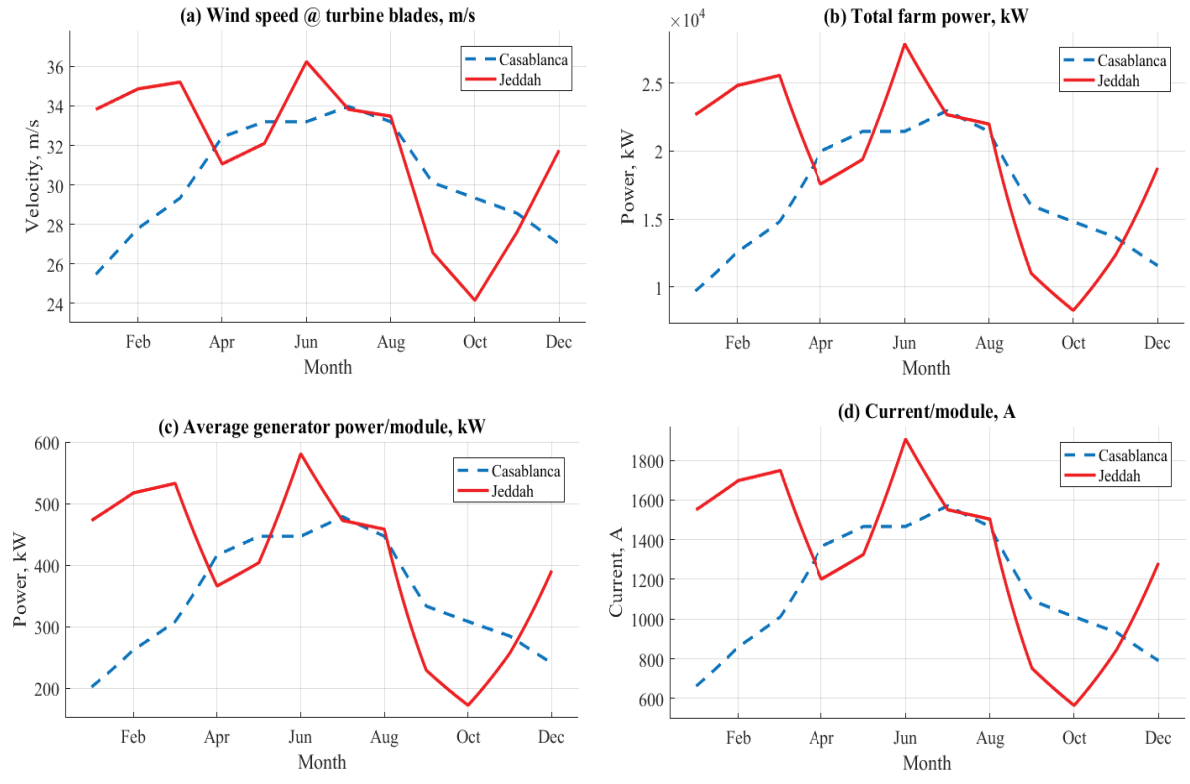

Fig. 6. The performance results of the HWT farm according to each location.

Fig. 7. represents the performance results of RO desalination plant at the locations of operations (Casablanca and Jeddah) during the whole year; it is the user power (kW), the total RO productivity (m^3/d), the feed flow rate (m^3/d), the product salinity (g/kg), the average brine salinity ratio (g/kg).

Fig. 7a perfectly shows that more than 50% of the power produced by the solar system has been sent to the end user, in the case of Casablanca, this power varies between ~1.4 kW in January and ~7 MW in June, in the case of Jeddah, the user power exceeds 8 MW in July where the irradiation is maximum. Concerning freshwater production (Fig. 7b), Jeddah site represents a high productivity compared to that of Casablanca, in Jeddah, this productivity varies between ~4,100 and ~13,810 m^3/d, and between ~1,900 and ~12,000 m^3/d. For this reason, the unit of RO requires a high feed flow rate, this flow rate in Jeddah city varies between ~1.2×10^4 and ~3.96×10^4 m^3/d, in Casablanca the feed flow rate varies also between ~0.52×10^4 and ~3.45×10^4 m^3/d (Fig. 7c). During the production of fresh water, their quality changes depending on the irradiation of the studied site (Fig. 7d), they are inversely proportional,

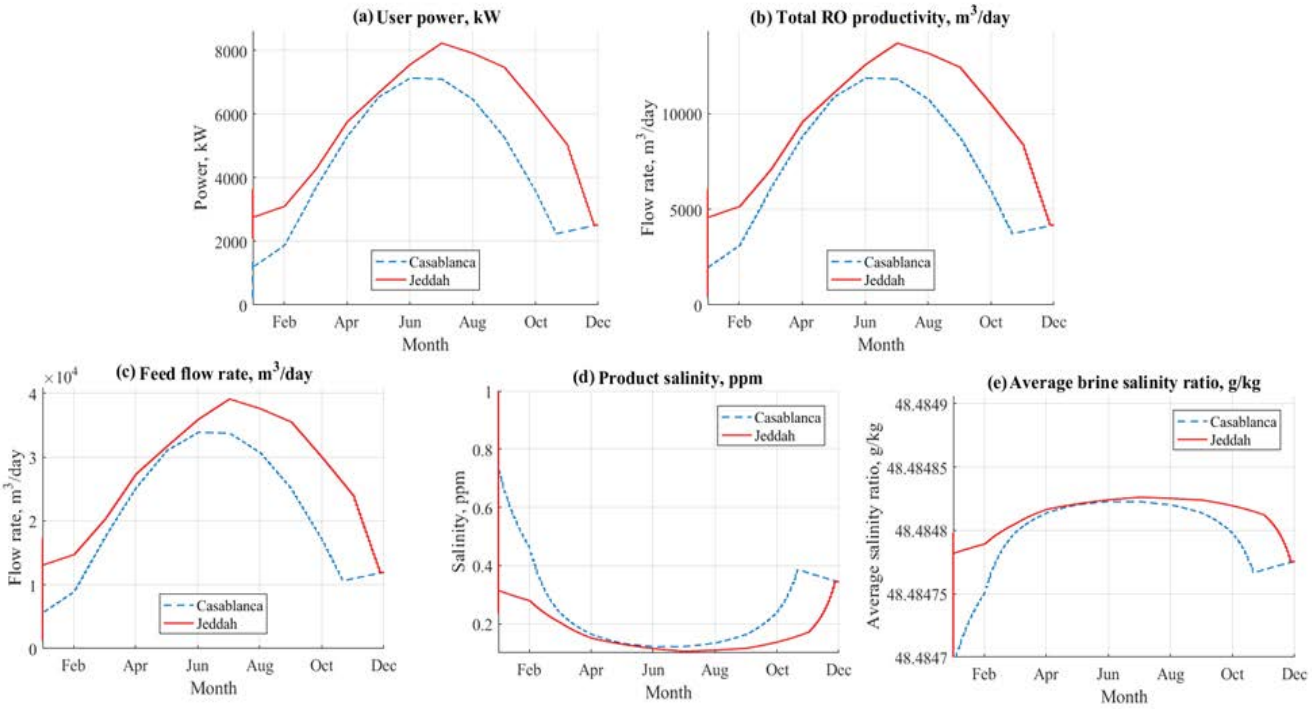

Fig. 7. Performance results for the RO desalination plant at the locations of operations (Casablanca and Jeddah).

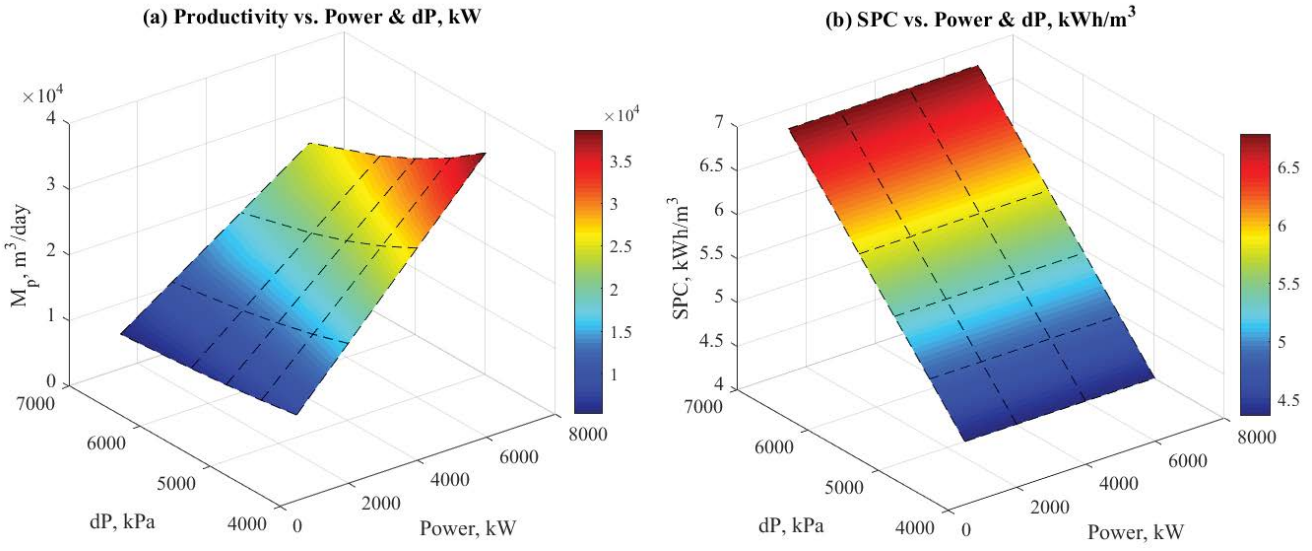

Fig. 8. The RO results according to the daily productivity and SPC based on the variation of power and pressure across the RO.

Table 2
The performance data results for the SCPP/HWT/RO system

Parameter	Casablanca, Morocco	Jeddah, KSA
Annual average GHI (W/m²)	520	780
Annual average ambient temperature (°C)	25	25
Annual average wind speed (m/s)	3.9	4.1
SCPP		
Air temperature entering the chimney (°C)	52.75	58.48
SCPP net output power (kW)	6,015	9,348
Thermal power to the air collector (kW)	13,780	20,780
Overall heat losses (W/m².°C)	1.368	1.401
Air mass flow rate (kg/s)	748.4	853
Air velocity at tower entrance (m/s)	8.567	9.853
Wind turbine rotor velocity (m/s)	15.94	18.25
Air pressures drop (Pa)	39.71	51.61
Total SCPP efficiency	0.588	0.586
Tower efficiency	0.7757	0.7689
Collector efficiency	0.9475	0.9526
HWT		
Wind speed at the turbine blades (m/s)	32.65	34.33
Air mass flow rate (kg/s)	4.138e4	4.35e4
Rotor swept area (m²)	3,491	3,491
Axial force (kN)	180.2	199.1
Power coefficient	0.252	0.252
Wind power/turbine (kW)	1,986	2,307
Mech power/turbine (kW)	500.4	581.4
Output generator power/turbine (kW)	425.3	494.2
Net developed power/turbine (kW)	453.6	527
Total farm power (kW)	2.268e4	2.635e4
Generator current/turbine (A)	1,395	1,621
Spacing in wind direction (m)	800	800
Spacing cross the wind direction (m)	200	200
Farm total area (km²)	8	8
RO		
Input power (kW)	6,804	7,905
User power (kW)	1.588e4	1.845e4
Specific power consumption (kWh/m³)	6.181	6.181
Productivity (m³/d)	2.642e4	3.07e4
Feed water flow rate (m³/d)	7.549e4	8.77e4
Brine flow rate (m³/d)	4.907e4	5.701e4
Brine salinity ratio (g/kg)	61.54	61.54
Product salinity (ppm)	54.45	46.86
Salt rejection	0.99	0.99
Total membranes area (m²)	18,532.5	18,532.5

therefore, in the region that deposits a high irradiation represents an important quality of freshwater, considering that the period when the irradiation is very high in Jeddah and Casablanca (April–October), the salinity of the production does not exceed 0.1 g/kg, on the other hand this salinity can reach a maximum of 0.75 g/kg in January in Casablanca and 0.35 g/kg in December in Jeddah. At the level of brine salinity ratio, their average value practically varies in a negligible way during the period of operating system, and their location too (Casablanca and Jeddah) Fig. 7e, this average brine salinity ratio is around 48.48 g/kg.

Fig. 8 shows the RO results according to the daily productivity and SPC based on the variation of power and pressure across the RO. Fig. 8a shows clearly that the effect of

varying the power and pressure across the RO unit on the daily productivity Mp, m^3/d by increasing the power and pressure will increase the productivity of the RO unit; in fact, this increase influences directly the SCP, kWh/m^3, of the system (Fig. 8b), which will increase this parameter, in fact, it becomes very important to find an optimal operation adopted at high production with low specific power consumption, which will minimize the total cost of produced water.

Table 2 represents the results and performance data of the SCPP/HWT/RO system in Casablanca, Morocco and Jeddah, KSA locations, at the same operating temperature (25°C), generally, the Jeddah site represents an important solar field and wind compared to that of Casablanca with an annual monthly average irradiation of the order of 780 W/m^2 (520 W/m^2 in Casablanca site), and an average monthly wind speed of 4.1 m/s (3.9 m/s in Casablanca site), for this reason, the overall operating performance of the whole systems (RO/SCPP/HWT) in the Jeddah city is very high compared to that of Casablanca, regarding the specific power consumption, the two sites require the same specific power value (6.181 kWh/m^3), with the production of two sites, this specific power consumption is still very high.

4. Conclusions

The aim of this study that has been executed is the combination of seawater desalination system, it is about the reverse osmosis desalination system assisted by solar chimney power plant and horizontal wind turbine (RO/SCPP/HWT), with the objective of producing electricity and freshwater. This energy is not only directed to the reverse osmosis unit but also to the users via their injection into the local electricity network. A comparative study between the two cities which are geographically different was carried out, that recognize a very important water stress; on the other hand, they are characterized by a very important renewable energy potential on a global scale (solar energy/wind energy). Casablanca, Morocco is a city in North Africa, and the other in the Arabian Gulf region is Jeddah, KSA.

This study demonstrates that the functional performance of the RO/SCPP/HWT system for a production of 3,500–10,500 m^3/d of freshwater and 10 MW e of electricity in the city of Jeddah, KSA are very high compared to that of Casablanca, Morocco. This difference is largely proportional to the methodological conditions of the two studied regions. Therefore, Jeddah, KSA has a very important energy and wind deposit than Casablanca, the thing that influences the production of freshwater and electricity to users. In this production system, the specific power consumption is high proportionally (6.181 kWh/m^3), and consequently the production cost will also be high, which requires optimization, and this will be the subject of the next work "the performance optimization of RO/SCPP/HWT system".

Symbols

A	—	Area, m^2
ASR	—	Air speed ratio
BS	—	Battery storage, Wh
c_p	—	Power coefficient, #
C_{pa}	—	Specific heat capacity, kJ/kg·°C at constant pressure
D	—	Diameter, m
d	—	Difference, #
DOD	—	Battery depth of discharge
Ec	—	Radiation to the ambient from the collector, W/m^2·K
Fx	—	Axial force, N
H	—	Height, m, elevation, m
hcr	—	Convection from the collector to the ambient, W/m^2·K
HHP	—	High pressure pump, kW
HP	—	Power, kW
I	—	Current, A
IF	—	Ideality factor
Is	—	Solar radiation, W/m^2
LF	—	Load factor, %
M	—	Mass flow rate, m^3/h, kg/s
N, n	—	Number, #
NOB	—	Number of batteries, #
NOC	—	Number of cloudy ds
NOM	—	Number of modules, #
OH	—	Operating h, h
P	—	Power, kW, or pressure, bar
ppm	—	Parts per million
Q	—	Useful air power, W
Qrr, Ql	—	Thermal losses, W
Qs	—	Solar thermal power, W
RO	—	Reverse osmosis
RPM	—	Rotor speed, tr/s
RR	—	Recovery ratio
SPC	—	Specific power consumption, kWh/m^3
SR	—	Salt rejection
SW	—	Seawater
T	—	Temperature, °C
t	—	Time, h
TBP	—	Total battery bank power, kW
TCF	—	Temperature correction factor, °C
TFP	—	Total Farm power, kW
Torg	—	Generator torque, N·m
Tort	—	Rotor torque, N·m
TSR	—	Tip speed ratio, #
Ul	—	Heat transfer coefficients, W/m^2·°C
V	—	Wind speed, m/s, voltage, V, air velocity, m/s
W	—	Rotor speed, rd/s
X	—	Salinity ratio, g/kg (ppm)
Xs	—	Optimum spacing in the wind direction, m
Y	—	Extraction percentage, %
Ys	—	Optimum spacing in cross wind direction, m

Subscripts

a, air	—	Air
am	—	Ambient
av	—	Average
b	—	Brine, battery
ch	—	Chimney
col, ac, c	—	Collector
d	—	Distillate product, discharge

e	—	Element
f	—	Feed
go, *g*	—	generator
l	—	Load
mec	—	Mechanical
nd, net	—	Net
p	—	Product or pump
r	—	Rotor
s	—	Site, solar
th	—	Thermal
Total, *t*	—	Total
u	—	Blades
v	—	pressure vessels
w	—	Water, wind
wt	—	Wind turbine

Greek

Δ	—	Difference
η	—	Efficiency, %
ρ	—	Density, kg/m^3
π	—	Osmotic pressure, kPa, number, #
α	—	Optical collector performance
σ	—	Stefan-Boltzmann constant (=5.67 × 10^{-8} W/m^2·k^4)

References

[1] UNICEF, MENA Report, Running Dry: The Impact of Water Scarcity on Children in the Middle East and North Africa, United Nations International Children's Emergency Fund, 2021. Available at: https://www.unicef.org/press-releases/running-dry-unprecedented-scale-and-impact-water-scarcity-middle-east-and-north

[2] A.O. Oliver, O.K. Overen, E.L. Meyer, Monthly, seasonal and yearly assessments of global solar radiation, clearness index and diffuse fractions in Alice, South Africa, Sustainability, 13 (2021) 2135, doi: 10.3390/su13042135.

[3] Y. Aroussy, D. Saifaoui, A. Lilane, Exergetic and thermo-economic analysis of different multi-effect configurations powered by solar power plants, Desal. Water Treat., 235 (2021) 26–38.

[4] A.A. Mabrouk, A.S. Nafey H.E.S. Fath, Thermoeconomic analysis of some existing desalination processes, Desalination, 205 (2007) 354–373.

[5] A.N. Mabrouk, H.S. Fath, Experimental study of high-performance hybrid NF-MSF by renewable energy, Desal. Water Treat., 51 (2013) 6895–6904 .

[6] M.A. Darwish, H.K. Abdulrahim, A.S. Hassan, A.A. Mabrouk, PV and CSP solar technologies and desalination: economic analysis, Desal. Water Treat., 57 (2016) 16679–16702.

[7] G. Iaquaniello, A. Salladini, A.A. Mabrouk, H.E.S. Fath, Concentrating solar power (CSP) system integrated with MED-RO hybrid desalination, Desalination, 336 (2014) 121–128.

[8] A.M. Soliman, A. Al-Falahi, M.A. Sharaf Eldean, M. Elmnifi, M. Hassan, B. Younis, A. Mabrouk, H.E.S. Fath, A new system design of using solar dish-hydro combined with reverse osmosis for sewage water treatment: case study Al-Marj, Libya, Desal. Water Treat., 193 (2020) 189–211.

[9] S.M. Alirahmi, S.R. Dabbagh, P. Ahmadi, S. Wongwises, Multi-objective design optimization of a multi-generation energy system based on geothermal and solar energy, Energy Convers. Manage., 205 (2020) 112426, doi: 10.1016/j.enconman.2019.112426.

[10] A.S. Nafey, M.A Sharaf, Combined solar organic Rankine cycle with reverse osmosis desalination process: energy, exergy, and cost evaluations, Renewable Energy, 35 (2010) 2571–2580.

[11] M.A. Sharaf, Thermo-economic comparisons of different types of solar desalination processes, J. Sol. Energy Eng., 134 (2012) 031001 (10 pages), doi: 10.1115/1.4005752.

[12] A.M. Delgado-Torres, L. García-Rodríguez, V.J. Romero-Ternero, Preliminary design of a solar thermal-powered seawater reverse osmosis system, Desalination, 216 (2007) 292–305.

[13] A. Lilane, D. Saifaoui, S. Hariss, H. Jenkal, M. Chouiekh, Modeling and simulation of the performances of the reverse osmosis membrane, Mater. Today: Proc., 24 (2020) 114–118.

[14] D.T. Agustín, G.R. Lourdes, Status of solar thermal-driven reverse osmosis desalination, Desalination, 216 (2007) 242–251.

[15] D.T. Agustín, G.R. Lourdes, Comparison of solar technologies for driving a desalination system by means of an organic Rankine cycle, Desalination, 216 (2007) 276–291.

[16] G.R. Lourdes, D.T. Agustín, Solar-powered Rankine cycles for freshwater production, Desalination, 212 (2007) 319–327.

[17] O. Charrouf, A. Betka, S. Abdeddaim, A. Ghamri, Artificial neural network power manager for hybrid PV-wind desalination system, Math. Comput. Simul., 167 (2020) 443–460.

[18] A.A. Monjezi, Y. Chen, R. Vepa, A. El-Hady B. Kashyout, G. Hassan, H. El-Banna Fath, A. El-Wahab Kassem, M.H. Shaheed, Development of an off-grid solar energy powered reverse osmosis desalination system for continuous production of freshwater with integrated photovoltaic thermal (PVT) cooling, Desalination, 495 (2020) 114679, doi: 10.1016/j.desal.2020.114679.

[19] W. Delgado, T. Beach, S.L. Beach, Solar rich and water poor: the case for solar desalination in El Paso, Texas, Prof. Geogr., 72 (2020) 9–21.

[20] X. Lai, R. Long, Z. Liu, W. Liu, Solar energy powered high-recovery reverse osmosis for synchronous seawater desalination and energy storage, Energy Convers. Manage., 228 (2021) 113665, doi: 10.1016/j.enconman.2020.113665.

[21] B. Martin-Gorriz, J.F. Maestre-Valero, B. Gallego-Elvira, P. Marín-Membrive, P. Terrero, V. Martínez-Alvarez, Recycling drainage effluents using reverse osmosis powered by photovoltaic solar energy in hydroponic tomato production: environmental footprint analysis, J. Environ. Manage., 297 (2021) 113326, doi: 10.1016/j.jenvman.2021.113326.

[22] A.S. Ibrahim, N. Fuentes, Z. He, R. Xin, K. Zuo, W.S. Walker, Q. Li, Treatment of brackish-water reverse osmosis brine using only solar energy, Environ. Sci. Water Res. Technol., 7 (2021) 1840–1851.

[23] S.E. Mohamed, G. Papadakis, E. Mathioulakis V. Belessiotis, A direct coupled photovoltaic seawater reverse osmosis desalination system toward battery-based systems-a technical and economical experimental comparative study, Desalination, 221 (2008) 17–22.

[24] A.M. Helal, S.A. Al-Malek, E.S. Al-Katheeri, Economic feasibility of alternative designs of a PV-RO desalination unit for remote areas in the United Arab Emirates, Desalination, 221 (2008) 1–16.

[25] A. Cipollina, E. Tzen, V. Subiela, M. Papapetrou, J. Koschikowski, R. Schwantes, M. Wieghaus, G. Zaragoza, Renewable energy desalination: performance analysis and operating data of existing RES desalination plants, Desal. Water Treat., 55 (2015) 3120–3140.

[26] M. Freire-Gormaly, A. Bilton, An experimental system for characterization of membrane fouling of solar photovoltaic reverse osmosis systems under intermittent operation, Desal. Water Treat, 73 (2017) 54–63.

[27] M. Freire-Gormaly, A. Bilton, Experimental quantification of the effect of intermittent operation on membrane performance of solar powered reverse osmosis desalination systems, Desalination, 435 (2018) 188–197.

[28] D. Manolakos, E. Sh. Mohamed, I. Karagiannis, G. Papadakis, Technical and economic comparison between PV-RO system and RO-Solar Rankine system. Case study: Thirasia island, Desalination, 221 (2008) 37–46.

[29] A.A. Hossam-Eldin, K.A. Abed, K.H. Youssef, H. Kotb, Technoeconomic optimization and new modeling technique of PV-wind-reverse osmosis desalination plant at variable load conditions, Int. J. Environ. Sci. Dev., 10 (2019) 223–230.

[30] E. Tzen, K. Perrakis, P. Baltas, Design of a standalone PV-desalination system for rural areas, Desalination, 119 (1998) 327–334.
[31] C.C.K. Liu, W. Xia, J.W. Park, A wind-driven reverse osmosis system for aquaculture wastewater reuse and nutrient recovery, Desalination, 202 (2007) 24–30.
[32] A. Lilane, D. Saifaoui, Y. Aroussy, S. Hariss, M. Oulhazzan, Experimental study of a pilot membrane desalination system: the effects of transmembrane pressure, Mater. Today Proc., 30 (2020) 970–975.
[33] I.N. Pestana, F.J.G. Latorre, C.A. Espinoza, A.G. Gotor, Optimization of RO desalination systems powered by renewable energies. Part I: wind energy, Desalination, 160 (2004) 293–299.
[34] D.A. Dehmas, N. Kherba, F.B. Hacene, N.K. Merzouk, M. Merzouk, H. Mahmoudia, M.F.A. Goosen, On the use of wind energy to power reverse osmosis desalination plant: a case study from Ténès (Algeria), Renewable Sustainable Energy Rev., 15 (2011) 956–963.
[35] T.P. Fluri, J.P. Pretorius, C. Van Dyk, T.W. Von Backström, D.G. Kröger, G. Van Zijl, Cost analysis of solar chimney power plants, Sol. Energy, 83 (2009) 246–256.
[36] K. Rahbar, A. Riasi, Performance enhancement and optimization of solar chimney power plant integrated with transparent photovoltaic cells and desalination method, Sustainable Cities Soc., 46 (2019) 101441, doi: 10.1016/j.scs.2019.101441.
[37] C. Méndez, Y. Bicer, Integration of solar chimney with desalination for sustainable water production: a thermodynamic assessment, Case Stud. Therm. Eng., 21 (2020) 100687, doi: 10.1016/j.csite.2020.100687.
[38] A. Alkhalidi, Y.K. Al-Jraba'ah, Solar desalination tower, novel design, for power generation and water distillation using steam only as working fluid, Desalination, 500 (2021) 114892, doi: 10.1016/j.desal.2020.114892.
[39] P. Rahdan, A. Kasaeian, W.M. Yan, Simulation and geometric optimization of a hybrid system of solar chimney and water desalination, Energy Convers. Manage., 243 (2021) 114291, doi: 10.1016/j.enconman.2021.114291.
[40] C. Méndez, Y. Bicer, Integrated system based on solar chimney and wind energy for hybrid desalination via reverse osmosis and multi-stage flash with brine recovery, Sustainable Energy Technol. Assess., 44 (2021) 101080, doi: 10.1016/j.seta.2021.101080.
[41] J. Li, P.-h. Guo, Y. Wang, Effects of collector radius and chimney height on power output of a solar chimney power plant with turbines, Renewable Energy, 47 (2012) 21–28.
[42] P. Guo, J. Li, Y. Wang, Numerical simulations of solar chimney power plant with radiation model, Renewable Energy, 62 (2014) 24–30.
[43] J. Schlaich, R. Bergermann, W. Schiel, G. Weinrebe, Design of commercial solar updraft tower systems—utilization of solar induced convective flows for power generation, J. Sol. Energy Eng., 127 (2005) 117–124.
[44] M.T. Sakir, M.B.K. Piash, M.S. Akhter, Design construction and performance test of a small solar chimney power plant, Global J. Res. Eng., 14 (2014) 2249–4596.
[45] M.A. Sharaf Eldean, A. El Shahat, A.M. Soliman, A new modeling technique based on performance data for photovoltaic modules and horizontal axis wind turbines, Wind Eng., 42 (2018) 209–229.
[46] M.R. Patel, O. Beik, Wind and Solar Power Systems: Design, Analysis, and Operation, CRC Press, 2021.
[47] G.N. Tiwari, S. Dubey, Fundamentals of Photovoltaic Modules and Their Applications, Royal Society of Chemistry Cambridge, 2010, 1757–6741.
[48] G. Amy, N. Ghaffour, Z. Li, L. Francis, R.V. Linares, T. Missimer, S. Lattemann, Membrane-based seawater desalination: present and future prospects, Desalination, 401 (2017) 16–21.
[49] A. Roy, S. Moulik, R. Kamesh, A. Mullick, Modeling in Membranes and Membrane-Based Processes, John Wiley & Sons, 2020.
[50] A. Lilane, D. Saifaoui, Y. Aroussy, M. Chouiekh, M.A. Sharaf-Eldean, A. Mabrouk, Simulation and optimization of pilot reverse osmosis desalination plant powered by photovoltaic solar energy, Desal. Water Treat., 258 (2022) 16–42.
[51] A. Lilane, D. Saifaoui, S. Ettami, M. Chouiekh, Y. Aroussy, Simulation and optimization of a RO/EV pilot reverse osmosis desalination plant powered by PV solar energy: the application to brackish water at low concentration, Eur. Phys. J. Appl. Phys., 97 (2022) 82, doi: 10.1051/epjap/2022220109.